Harnessing Surface Plasmons for Magnetic Resonance Imaging Applications

Carlo Rizza,[1,2,*] Marco Fantasia,[3] Elia Palange,[4] Marcello Alecci,[2,3,5] and Angelo Galante[2,3,5]

[1] *Department of Physical and Chemical Sciences, University of L'Aquila, Via Vetoio 1, 67100 L'Aquila, Italy*

[2] *Institute for Superconductors, Oxides and Other Innovative Materials and Devices (SPIN), National Research Council (CNR), Via Vetoio 1, 67100 L'Aquila, Italy*

[3] *Department of Life, Health and Environmental Sciences (MESVA), University of L'Aquila, Via Vetoio 1, 67100 L'Aquila, Italy*

[4] *Department of Industrial and Information Engineering and Economics, University of L'Aquila, Via G. Gronchi 18, 67100 L'Aquila, Italy*

[5] *Laboratori Nazionali del Gran Sasso, Istituto Nazionale di Fisica Nucleare, 67000 Assergi, L'Aquila, Italy*

(Received 19 March 2019; revised manuscript received 21 June 2019; published 10 October 2019)

Highly localized electromagnetic waves appearing in subwavelength structures, such as surface plasmons lying on a metal surface, are fundamental ingredients in nanophotonics since they offer novel routes for advanced subwavelength light control. Negative-magnetic-permeability metamaterials, already proposed for nuclear magnetic resonance imaging (MRI) applications, can also support magnetic-surface-plasmon excitations. Here we propose to exploit this phenomenon to increase MRI efficiency. We show that a negative-magnetic-permeability metamaterial slab, coupled to a standard radio-frequency surface coil, supports highly localized magnetic surface plasmons, allowing us to boost and to spatially manipulate the radio-frequency electromagnetic field. Our predictions indicate that the configuration considered holds great potential to enhance the MRI signal-to-noise ratio with respect to standard setups.

DOI: 10.1103/PhysRevApplied.12.044023

I. INTRODUCTION

Surface plasmons (i.e., light-induced collective electronic excitations lying at a planar dielectric-metal interface) are fundamental ingredients in the field of nanophotonics. These excitations display several significant characteristics; for example, a resonant nature and strong enhancement and a high degree of confinement of the local electromagnetic field [1]. As such, surface plasmons have been exploited to achieve an enormous variety of applications, such as subwavelength waveguides [2], plasmonic lenses [3], and ultrasensitive biosensors and chemosensors [4]. In addition, over the last decade, metamaterials (viz., composite materials designed to achieve advantageous and/or unusual properties) provided an extraordinary platform for plasmon optics since they have large potential to manipulate the near-field electromagnetic response at will. As a significant example, metamaterial science allowed the design of a negative-magnetic-permeability medium [5–7] and the observation of the unusual magnetic counterpart of surface plasmons (viz., magnetic surface plasmons [8,9]) excited at a dielectric-metamaterial interface. Indeed, negative magnetic permeability is a fundamental ingredient for realizing many fascinating electromagnetic devices, such as an invisibility cloak [10] and far-field hyperlensing [11].

In the context of magnetic resonance imaging (MRI), over the years the quest for signal increase has been focused on the boost of the static magnetic fields [12], improved designs for high-performance radio-frequency (rf) coils [13,14], or the inclusion of high-dielectric-constant pads [15]. More recently, several research groups have exploited the metamaterial concept to manipulate the rf field in MRI. Wiltshire *et al.* [16] proposed and experimentally realized microstructured magnetic materials (Swiss-roll arrays) to guide rf flux from an object to a remote receiver coil. Freire *et al.* [17] investigated a $\mathrm{Re}\,\mu_m = -1$ metamaterial (i.e., a metamaterial where the real part of the magnetic permeability is -1) coupled to a standard surface rf coil. In the latter, the slab behaves as a subdiffraction lens (Pendry lens) [18,19] able to refocus the rf magnetic field, such as to extend the field of view beyond the limits imposed by the standard approach. Recently, metasurfaces were exploited to locally increase MRI sensitivity [20–25]. The metasurface considered (viz., an array of metallic inclusions embedded in a dielectric medium) can support Fabry-Perot resonances, which are responsible for global redistribution and local enhancement of the rf electromagnetic field inside the sample.

*carlo.rizza@univaq.it

 © 2019 American Physical Society

In this paper, we go one step further and suggest the application of magnetic surface plasmons, excited at the surface of a $\mathrm{Re}\,\mu_m = -1$ metamaterial slab, in the context of MRI. For the first time to our knowledge, we show that the resonant nature of magnetic surface plasmons can be suitably exploited to increase MRI efficiency. We consider a $\mathrm{Re}\,\mu_m = -1$ metamaterial slab embedded in a MRI setup as depicted in Fig. 1. In this configuration, we show that the metamaterial supports magnetic surface plasmons and their excitations can boost the MRI signal-to-noise ratio (SNR) with respect to the standard setup. It is surprising that a $\mathrm{Re}\,\mu_m = -1$ metamaterial is able to support both a Pendry lens (exploited by Freire *et al.* [17] for MRI applications) and surface-plasmon exicitations, even though they are different phenomena [18]. In the setup considered by Freire *et al.*, the $\mathrm{Re}\,\mu_m = -1$ slab is located between the coil and the sample and it is able to reproduce in a plane inside the sample the same electromagnetic field configuration present on the rf-coil surface (when suitable conditions pertaining to the metamaterial thickness and its distance from the coil are satisfied). In contrast, well-defined surface plasmons can be excited near the boundary of a semi-infinite $\mathrm{Re}\,\mu_m = -1$ metamaterial and they yield a strong resonance enhancement of the local electromagnetic field. The paper is organized as follows. In Sec. II, we investigate the MRI setup reported in Fig. 1, where a $\mathrm{Re}\,\mu_m = -1$ metamaterial, supporting magnetic surface plasmons, is considered and we evaluate the rf magnetic field and SNR enhancement due to excitation of magnetic surface plasmons. In Sec. III, we obtain the conditions for achieving excitation of surface plasmons . In Sec. IV, we discuss the enhancement of the rf-coil transmitted signal. In Sec. V, we draw our conclusions.

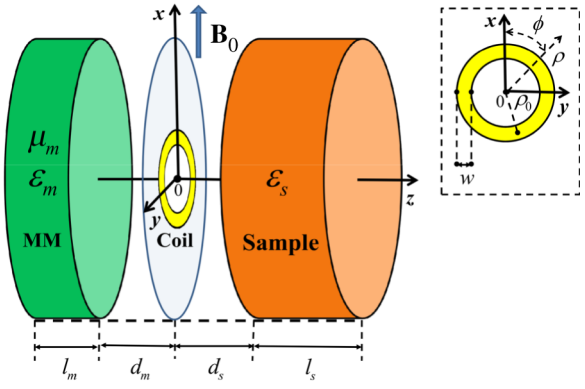

FIG. 1. The setup considered. A standard surface rf coil (with radius ρ_0 and radial width w) at $z = 0$ is positioned between the metamaterial (MM) slab (with thickness l_m, relative permittivity ϵ_m, and permeability μ_m) and the sample (with thickness l_s and relative permittivity ϵ_s). $\mathbf{B}_0$ is the applied static magnetic field and d_m (d_s) is the distance between the metamaterial (the sample) and the rf coil.

II. EXCITATION OF MAGNETIC SURFACE PLASMONS AND SNR ENHANCEMENT

In the attempt to exploit the high local fields associated with surface plasmons by keeping the surface rf coil as close as possible to the sample, we suggest the configuration depicted in Fig. 1, where the rf coil is located between the metamaterial slab and the sample. In the situation where the metamaterial–rf-coil and the rf-coil–sample distances are small ($d_m \simeq d_s \simeq 0$ cm) and the metamaterial thickness is large (compared with the rf-coil size), we expect that the $\mathrm{Re}\,\mu_m = -1$ metamaterial slab supports magnetic surface plasmons, which are tightly localized around its surface and they provide a high resonance enhancement of the electromagnetic field inside the sample. Performing suitable full-wave simulations [26], we investigate the configuration shown in Fig. 1 and hence we evaluate the spatial distribution of the rf magnetic field and the MRI SNR. In the numerical examples, we set the frequency $\nu = \nu_0 = 63.866$ MHz (where ν_0 is the Larmor frequency corresponding to a static magnetic field $|\mathbf{B}_0| = 1.5$ T), $l_m = 5.7$ cm as in [19], $l_s = 20$ cm, $d_m = 0$ mm, either $d_s = 0$ mm or $d_s = 4$ mm, the sample relative permittivity $\epsilon_s = 90 + i197$ (corresponding to the average of human-tissue values and conductivity $\sigma = 0.69$ S/m), and the metamaterial relative permittivity $\epsilon_m = 1$.

The rf surface coil is modeled with negligible thickness along the z axis and by a surface current density having only an azimuthal component; that is, $J_\phi = K_\phi \delta(z)$, where $K_\phi(\rho) = K_0 \rho \exp[-(\rho - \rho_0)^2/w^2]$ ($\rho_0 = 2$ cm, $w = 2$ mm, K_0 is a constant whose value is fixed to obtain unitary current) and $\delta(\cdot)$ is the Dirac δ function. The assumed current-density distribution is an approximation of the real one, which will be peaked at the edges of the rf coil, but is a useful model to catch the main physical consequences of the surface-plasmon excitations. Since the circular rf coil is approximated with a given current-density profile, in the following, we do not consider the rf-coil losses and focus on losses inside the sample and the metamaterial slab only (see Supplemental Material [27] for further details on simulations).

In an MRI setup, the receiving-rf-coil signal is given by $S \propto |B_1^{(-)}(\rho, \phi, z)|$, where $B_1^{(-)}$ is the complex amplitude of the counter-rotating transverse rf magnetic field (orthogonal to the static magnetic field $\mathbf{B}_0$) produced by the coil per unit current. Considering the geometry displayed in Fig. 1, where $\mathbf{B}_0$ is along the x axis, we obtain $B_1^{(-)} = (B_{1\rho} \sin\phi + iB_{1z})/2$, where the rf magnetic field in cylindrical coordinates is given by $\mathbf{B}_1(\rho, \phi, z) = \mathrm{Re}\left[\left(B_{1\rho}\hat{\rho} + B_{1z}\hat{\mathbf{z}}\right) e^{-i\omega t}\right]$, where $\omega = 2\pi\nu$ (see Supplemental Material [27]). On the other hand, the noise is proportional to the square root of the dissipated power P in the system, so the receiving-rf-coil SNR is proportional to $B_1^{(-)}|/\sqrt{P}$ [28–30]. If we ignore the rf-coil losses [19], the dissipated power is approximated as $P = P_s + P_m$, where P_s and P_m are the dissipated

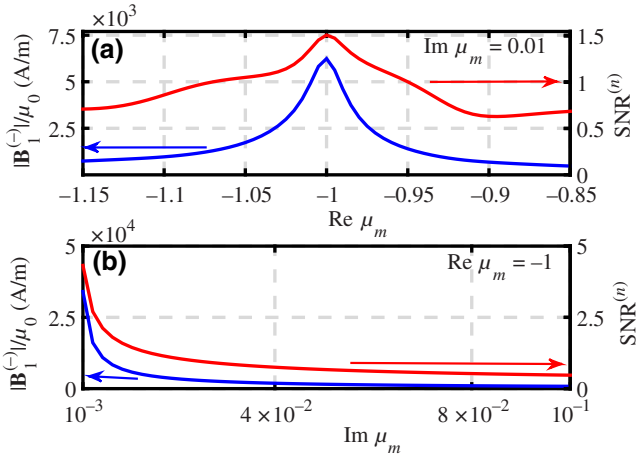

FIG. 2. The rf magnetic field per unit current $|B_1^{(-)}|/\mu_0$ (blue lines) and the normalized SNR (SNR$^{(n)}$) (red lines) as a function of Re μ_m [with Im $\mu_m = 10^{-2}$ in (a)] and Im μ_m [with Re $\mu_m = -1$ in (b)], respectively. Both $|B_1^{(-)}|/\mu_0$ and the normalized SNR are evaluated at the point $\rho = 2$ cm, $\phi = \pi/2$, and $z = 1$ mm, and we set $d_s = 0$ mm.

power in the sample and the metamaterial, respectively. To highlight the advantages related to the presence of the metamaterial slab, in the following we consider the normalized signal-to-noise ratio $\mathrm{SNR}^{(n)} = \mathrm{SNR}_m/\mathrm{SNR}_v$, where SNR_m and SNR_v are the values calculated with and without the metamaterial slab (v stands for "vacuum"), respectively. In Fig. 2, we report $|B_1^{(-)}|/\mu_0$ (blue lines) and the normalized SNR (red lines) for different values of the metamaterial permeability μ_m at the coordinate point $\rho = 2$ cm, $\phi = \pi/2$, and $z = 1$ mm. In Fig. 2(a) we have set $\mathrm{Im}\,\mu_m = 0.01$ and $\mathrm{Re}\,\mu_m$ spans the range from -1.15 to -0.85. In Fig. 2(b), we have considered $\mathrm{Re}\,\mu_m = -1$ and $\mathrm{Im}\,\mu_m$ spans the range from 10^{-3} to 10^{-1}. As expected, the magnetic field in Fig. 2 shows a resonant behavior and, more importantly, the normalized SNR becomes greater than 1 at the resonance condition (e.g., normalized SNR of approximately 5 for $\mu_m = -1 + i10^{-3}$).

III. THE PLASMONIC REGIME

To physically grasp the role played by surface plasmons and hence their relevance for the results shown in Fig. 2, we analytically solve Maxwell's equations in the previously considered configuration, where the only change is that the sample is a semi-infinite slab (i.e., $l_s \to \infty$) (see Supplemental Material [27]). Exploiting the system rotational symmetry around the z axis, we find the complex amplitudes of the electric and magnetic fields are $\mathbf{E}_\phi = i\omega\mathbf{A}_\phi$ and $\mathbf{B}_1 = \nabla \times \mathbf{A}_\phi$, where $\mathbf{A}_\phi$ is the azimuthal component of the electromagnetic vector potential, and we search for solutions of Maxwell's equations by using the Hankel transform $A_\phi(\rho, z) = \int_0^{+\infty} dk_\rho k_\rho J_1(k_\rho \rho)\, \tilde{A}_\phi(k_\rho, z)$. In the static limit, one can highlight two different regimes:

(a) The Pendry regime, where a $\mathrm{Re}\,\mu_m = -1$ metamaterial slab can behave as a Pendry lens in the situation where the current-density spatial spectrum $\tilde{K}_\phi(k_\rho)$ lies in the region $k_\rho \ll k_1$,

(b) The plasmonic regime, where a $\mathrm{Re}\,\mu_m = -1$ metamaterial slab supports surface-plasmon excitations in the situation where $\tilde{K}_\phi$ lies in the region $k_\rho \gg k_1$, where k_1 is related to the slab geometry and losses; that is, $k_1 = l_m^{-1} \log(2/\mathrm{Im}\,\mu_m)$.

In Pendry regime the complex amplitude of the vector potential is given by

$$A_\phi \simeq -\frac{\mu_0 \mu_m}{2} \int_0^{+\infty} dk_\rho J_1(k_\rho \rho)\, \tilde{K}_\phi e^{-k_\rho z}, \qquad (1)$$

whereas in the plasmonic regime we obtain

$$A_\phi \simeq \frac{\mu_0 \mu_m}{1 + \mu_m} \int_0^{+\infty} dk_\rho J_1(k_\rho \rho)\, \tilde{K}_\phi e^{-k_\rho z}. \qquad (2)$$

Pendry's mechanism holds for plane waves whose transverse wave number satisfies the condition $k_\rho \ll k_1$, and this corresponds to a minimum lens resolution $\Delta = 2\pi l_m/\log(2/\mathrm{Im}\,\mu_m)$ [31]. As a consequence, this regime is obtained with a surface loop with large diameter (e.g., like the one in Ref. [19]). On the other hand, if the rf coil is sufficiently reduced in size, a significant part of spatial spectrum can lie in the region $k_\rho \gg k_1$, where surface plasmons can be excited (roughly, the condition $k_\rho \gg k_1$ entails $\rho_0 \ll 2\pi/k_1$ [32]). In addition, Eqs. (1) and (2) hold only in the region $z > 0$ (i.e., inside the sample). It is worth noting that Eq. (1) with $\mu_m = -1$ coincides with the expression for the potential field in the case where the metamaterial is absent. As a consequence, in the Pendry regime and in the setup considered here, the metamaterial does not affect the spatial distribution of the electromagnetic field inside the sample. From Eq. (2), it is evident that one can achieve a very large enhancement of the field amplitude A_ϕ if the condition $\mathrm{Re}\,\mu_m = -1$ holds and $\mathrm{Im}\,\mu_m$ is sufficiently small. This quasi-pole condition corresponds to the existence of exponentially localized electromagnetic modes lying around the metamaterial surface at $z = 0$. If we consider the circular rf coil for MRI used for signal reception, the received-signal strength, as stated above, depends on the rf field $B_1^{(-)}$. As a consequence, we expect the latter to be significantly enhanced when a low-loss $\mathrm{Re}\,\mu_m = -1$ metamaterial is present. This enhancement is localized close to the metamaterial surface and its intensity is strongly dependent on the imaginary part of the relative permeability, with the smaller $\mathrm{Im}\,\mu_m$ providing the larger detected signal. The physical

mechanism considered here is very different from the one proposed by Pendry. The lens mechanism is due to the fact that evanescent waves show a nonintuitive exponential growth inside the metamaterial, so wave modes (satisfying the condition $k_\rho \ll k_1$) emitted by the source can be transmitted without diffraction for a suitable lens thickness. Surface plasmons lying at the metamaterial surface exist in the opposite regime (the plasmonic regime). In this regime, the $\mathrm{Re}\,\mu = -1$ metamaterial does not behave as a lens and it can produce a hyperfocusing of the electromagnetic field near the metamaterial surface.

To spatially visualize the mechanism, in Fig. 3 we report the spatial distribution of the normalized SNR with the same geometrical parameters used in Fig. 2. For $\mathrm{Im}\,\mu_m = 10^{-1}$, we get a significant spatial modulation of the normalized SNR, and the magnetic loss inside the metamaterial is responsible for an overall decreased performance of the receiving system (normalized SNR less than 1). If we set $\mathrm{Im}\,\mu_m = 10^{-3}$ ($\mathrm{Im}\,\mu_m = 10^{-2}$), although the noise is strongly affected by metamaterial losses, that is, $P_m/P_s \simeq 1$ ($P_m/P_s \simeq 3$), the resonant plasmon excitation entails a redistribution of the rf electromagnetic field [see Figs. 3(b) and 3(c)] and a strong local enhancement of the normalized SNR; that is, a normalized SNR of approximately 7.5 (approximately 2.5). From Fig. 3 it is evident that for the geometry considered if $\mathrm{Im}\,\mu_m \leq 10^{-3}$, the attainable normalized SNR in a MRI experiment with the proposed inclusion of a metamaterial slab can be increased by a large factor within at least a 1-cm sample depth and 7-cm lateral size. Standard rf surface coils are used to acquire images from a region of interest (ROI) positioned in front of the coil center. In our setup, we get a significant SNR enhancement in front of the coil as in the standard setup, although the penetration depth, along the coil axis, is limited to approximately 1 mm. However, as shown in Figs. 3(b) and 3(c), SNR increase is also obtained off-axis (up to 7 cm), and this could be useful in specific MRI applications, where the ROI is much larger than the coil size along the radial direction (e.g., cortical brain imaging). Moreover, the rf-coil positioning could be easily shifted so that the region of higher SNR matches the sample ROI. For completeness, in Fig. 3(d), we investigate the metamaterial setup where the distance between the rf coil and the sample d_s is 4 mm and $\mathrm{Im}\,\mu_m = 10^{-3}$. In this condition, a significant enhancement of the normalized SNR persists, with a spatial distribution similar to the one in Fig. 3(b), even if its maximum decreases with respect to the $d_s = 0$ mm configuration [Fig. 3(c)].

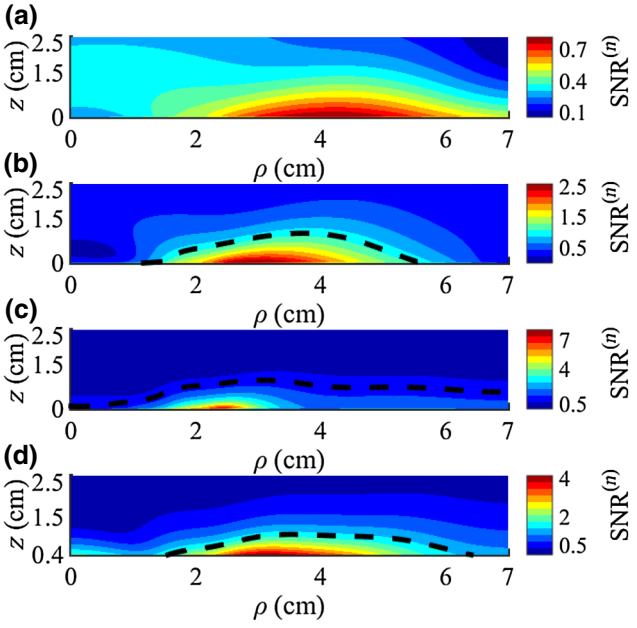

FIG. 3. Maps of the normalized SNR ($\mathrm{SNR}^{(n)}$) for $d_s = 0$ mm, $\phi = \pi/2$, and $\mathrm{Re}\,\mu_m = -1$ with $\mathrm{Im}\,\mu_m = 10^{-1}$ (a), $\mathrm{Im}\,\mu_m = 10^{-2}$ (b), and $\mathrm{Im}\,\mu_m = 10^{-3}$ (c). In (d), the same parameters as for (c) hold except $d_s = 4$ mm. The dashed black lines are contour lines for a normalized SNR of 1.

Loss reduction is the most challenging issue in metamaterial science. Generally, the desired negative permeability is achieved by means of a suitable periodic array of metallic inclusions such as split-ring resonators or wires. In these configurations, losses are given by Ohmic dissipation in the metallic components, and previous experimental realizations within the frequency range of interest for MRI do not satisfy the above requirement [17,33]. However, metamaterial design is a fast-growing field, and either superconductors [34] or high-dielectric-constant inclusions [35–37] can be suitable remedies for reducing losses. As an example, ferroelectric materials can show permittivity with a very high real part and a low imaginary part in the radio-frequency range [38], so they can be used as metamaterial inclusions for realizing the desired magnetic metamaterial structure. In addition, standard magnetic metamaterials can display strong frequency dispersion, and this effect can alter to some extent the predicted enhancement of the rf magnetic field in the setup considered. On the other hand, strong dispersion effects can be reduced by careful engineering of the metamaterial structure [39].

IV. TRANSMISSION ENHANCEMENT

To evaluate the impact of surface-plasmon excitations on the signal transmitted by a rf coil, we consider the spatial distribution of the transmit field $B_1^{(+)}$ inside the sample. The transmission signal depends on the complex amplitude of the corotating magnetic field per unit current; that is, $B_1^{(+)} = \left(B_{1\rho}\sin\phi - iB_{1z}\right)^*/2$. In Fig. 4 we plot the logarithm of the normalized magnetic field $|B_1^{(+,n)}| = |B_1^{(+)}|/|B_{1,v}^{(+)}|$ by setting $\phi = \pi/2$, where $|B_{1,v}^{(+)}|$ is the maximum of the absolute value of the magnetic corotating field per unit current inside the sample in the setup without the metamaterial slab. In Fig. 4(a), we report

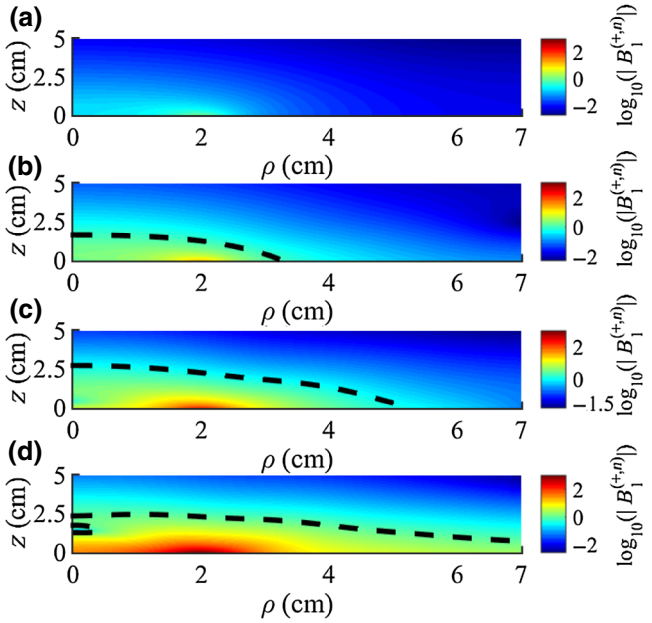

FIG. 4. $\log_{10}|B_1^{(+,n)}|$ maps with $d_s = 0$ mm and $\phi = \pi/2$ with $\mu_m = 1$ (a) (i.e., the configuration without the metamaterial) and with $\mu_m = -1 + i10^{-1}$ (b), $\mu_m = -1 + i10^{-2}$ (c), and $\mu_m = -1 + i10^{-3}$ (d). The dashed black lines are $\log_{10}|B_1^{(+,n)}| = 0$ contour lines.

$\log_{10}|B_1^{(+,n)}|$ inside the sample region in the absence of the metamaterial (i.e., $\mu_m = 1$), whereas in Figs. 4(b)–4(d), we plot $\log_{10}|B_1^{(+,n)}|$ for $\mathrm{Re}\,\mu_m = -1$ and different values of $\mathrm{Im}\,\mu_m$.

As expected from the theoretical analysis, the smaller $\mathrm{Im}\,\mu_m$, the greater is k_1 and hence the excited wave modes are more tightly confined near the sample-metamaterial interface, since the $\tilde{K}_\phi$ spectrum fraction in the plasmonic regime is reduced and the amplification prefactor increases [see Eq. (2)].

The net effects, as in Fig. 4, are the enhancement and the focusing of the rf magnetic field close to the current source. As a consequence, a first possible application of the setup considered is related to MRI signal transmission. The large attainable increase of the $|B_1^{(+)}|$ field can boost the transmission performances of the system, allowing much shorter rf pulses for a given flip angle. Such an effect can eventually be controlled when multiple surface transmit rf coils are available, allowing parallel transmission MRI techniques [40,41].

V. CONCLUSIONS

In conclusion, we suggest that a negative-permeability metamaterial embedded in a MRI setup can improve the performance of a rf coil in a MRI experiment. The approach is based on magnetic plasmon resonances present on the surface of a $\mathrm{Re}\,\mu_m = -1$ metamaterial slab, which is responsible for a large increase of the rf magnetic field within a sample suitable for MRI. Finally, we stress that the configuration geometry considered has the additional advantage of introducing no limitations on the sample–rf-coil relative position, so the present proposal has the potential to enhance the MRI signal-to-noise ratio with respect to standard setups, with minor additional requirements.

ACKNOWLEDGMENTS

This work was partially supported by the CNR-SPIN seed project no. B52F17001370005 and CNR-SPIN Nano-Agents project.

[1] A. V. Zayats, I. I. Smolyaninov, and A. A. Maradudin, Nano-optics of surface plasmon polaritons, Phys. Rep. **408**, 131 (2005).
[2] R. F. Oulton, V. J. Sorger, D. A. Genov, D. F. P. Pile, and X. Zhang, A hybrid plasmonic waveguide for subwavelength confinement and long-range propagation, Nat. Photonics **2**, 496 (2008).
[3] Y. Fu and X. Zhou, Plasmonic lenses: A review, Plasmonics **5**, 287 (2010).
[4] M. Li, S. K. Cushinga, and N. Wu, Plasmon-enhanced optical sensors: A review, Analyst **140**, 386 (2015).
[5] J. B. Pendry, A. J. Holden, D. J. Robbins, and W. J. Stewart, Magnetism from conductors and enhanced nonlinear phenomena, IEEE Trans. Microwave Theory Tech. **47**, 2075 (1999).
[6] S. Linden, C. Enkrich, M. Wegener, J. Zhou, T. Koschny, and C. M. Soukoulis, Magnetic response of metamaterials at 100 terahertz, Science **306**, 1351 (2004).
[7] C. Enkrich, M. Wegener, S. Linden, S. Burger, L. Zschiedrich, F. Schmidt, J. F. Zhou, T. Koschny, and C. M. Soukoulis, Magnetic Metamaterials at Telecommunication and Visible Frequencies, Phys. Rev. Lett. **95**, 203901 (2005).
[8] S. Zhang, W. Fan, B. K. Minhas, A. Frauenglass, K. J. Malloy, and S. R. J. Brueck, Midinfrared Resonant Magnetic Nanostructures Exhibiting a Negative Permeability, Phys. Rev. Lett. **94**, 037402 (2005).
[9] J. N. Gollub, D. R. Smith, D. C. Vier, T. Perram, and J. J. Mock, Experimental characterization of magnetic surface plasmons on metamaterials with negative permeability, Phys. Rev. B **71**, 195402 (2005).
[10] J. B. Pendry, D. Schurig, and D. R. Smith, Controlling electromagnetic fields, Science **312**, 1780 (2006).
[11] Z. Jacob, L. V. Alekseyev, and E. Narimanov, Optical hyperlens: Far-field imaging beyond the diffraction limit, Opt. Express **14**, 8247 (2006).
[12] W. Van Der Zwaag, A. Schäfer, J. P. Marques, R. Turner, and R. Trampel, Recent applications of UHF-MRI in the study of human brain function and structure: A review, NMR Biomed. **29**, 1274 (2016).
[13] H. Wen, F. A. Jaffer, T. J. Denison, S. Duewell, A. S. Chesnick, and R. S. Balaban, The evaluation of dielectric

resonators containing H_2O or D_2O as RF coils for high-field MR imaging and spectroscopy, J. Magn. Reson. B **110**, 117 (1996).

[14] S. A. Aussenhofer and A. G. Webb, Design and evaluation of a detunable water-based quadrature HEM_{11} mode dielectric resonator as a new type of volume coil for high field MRI, Magn. Reson. Med. **68**, 1325 (2012).

[15] J. Van Gemert, W. Brink, A. Webb, and R. Remis, High permittivity pad design tool for 7T neuroimaging and 3T body imaging, Magn. Reson. Med. **81**, 3370 (2019).

[16] M. C. K. Wiltshire, J. B. Pendry, I. R. Young, D. J. Larkman, D. J. Gilderdale, and J. V. Hajnal, Microstructured magnetic materials for RF flux guides in magnetic resonance imaging, Science **291**, 849 (2001).

[17] M. J. Freire, R. Marques, and L. Jelinek, Experimental demonstration of a $\mu = -1$ metamaterial lens for magnetic resonance imaging, Appl. Phys. Lett. **93**, 231108 (2008).

[18] J. B. Pendry, Negative Refraction Makes a Perfect Lens, Phys. Rev. Lett. **85**, 3966 (2000).

[19] M. J. Freire, L. Jelinek, R. Marques, and M. Lapine, On the applications of $\mu_r = -1$ metamaterial lenses for magnetic resonance imaging, J. Magn. Reson. **203**, 81 (2010).

[20] A. P. Slobozhanyuk, A. N. Poddubny, A. J. E. Raaijmakers, C. A. T. van den Berg, A. V. Kozachenko, I. A. Dubrovina, I. V. Melchakova, Y. S. Kivshar, and P. A. Belov, Enhancement of magnetic resonance imaging with metasurfaces, Adv. Mater. **28**, 1832 (2016).

[21] R. Schmidt, A. Slobozhanyuk, P. Belov, and A. Webb, Flexible and compact hybrid metasurfaces for enhanced ultra high field in vivo magnetic resonance imaging, Sci. Rep. **7**, 1678 (2017).

[22] R. Schmidt and A. Webb, Metamaterial combining electric- and magnetic-dipole-based configurations for unique dual-band signal enhancement in ultrahigh-field magnetic resonance imaging, ACS Appl. Mater. Interfaces **9**, 34618 (2017).

[23] A. V. Shchelokova, A. P. Slobozhanyuk, I. V. Melchakova, S. B. Glybovski, A. G. Webb, Y. S. Kivshar, and P. A. Belov, Locally Enhanced Image Quality with Tunable Hybrid Metasurfaces, Phys. Rev. Appl. **9**, 014020 (2018).

[24] A. A. Mikhailovskaya, A. V. Shchelokova, D. A. Dobrykh, I. V. Sushkov, A. P. Slobozhanyuk, and A. Webb, A new quadrature annular resonator for 3 T MRI based on artificial-dielectrics, J. Mag. Res. **291**, 47 (2018).

[25] A. V. Shchelokova, A. P. Slobozhanyuk, P. de Bruin, I. Zivkovic, E. Kallos, P. A. Belov, and A. Webb, Experimental investigation of a metasurface resonator for in vivo imaging at 1.5 T, J. Mag. Res. **286**, 78 (2018).

[26] COMSOL Group, COMSOL Multiphysics.

[27] See Supplemental Material at http://link.aps.org/supplemental/10.1103/PhysRevApplied.12.044023 for additional details on the numerical simulations, definitions of the rf-coil signal strengths in a MRI setup, and the analytical expression for the magnetic vector potential produced by the rf coil in the setup considered.

[28] E. M. Haacke, R. W. Brown, M. R. Thompson, and R. Venkatesan, *Magnetic Resonance Imaging: Principles and Sequence Design* (Wiley, New York, 1999).

[29] D. I. Hoult, The principle of reciprocity in signal strength calculations - a mathematical guide, Concepts Magn. Reson. **4**, 173 (2000).

[30] A. G. Webb, *Magnetic Resonance Technology: Hardware and System Component Design (New Developments in NMR* (The Royal Society of Chemistry, Cambridge, 2016). www.rsc.org.

[31] J. M. Algarin, M. J. Freire, M. A. Lopez, M. Lapine, P. M. Jakob, V. C. Behr, and R. Marqués, Analysis of the resolution of split-ring metamaterial lenses with application in parallel magnetic resonance imaging, Appl. Phys. Lett. **98**, 014105 (2011).

[32] Considering that to achieve a SNR enhancement, $\mathrm{Im}\,\mu_m$ ranges from about 10^{-3} to 2×10^{-2} [see Fig. 2(b)], $2\pi/k_1$ ranges from about 5 cm to 8 cm. In all simulations we choose a coil radius of 2 cm so that the condition $\rho_0 \ll 2\pi/k_1$ holds and resonant surface plasmons are excited. Note that in a number of preclinical and clinical MRI applications, surface coils with a diameter between about 1 and 8 cm are commonly used and the present configuration should be of interest.

[33] J. M. Algarin, M. J. Freire, F. Breuer, and V. C. Behr, Metamaterial magnetoinductive lens performance as a function of field strength, J. Mag. Res. **247**, 9 (2014).

[34] S. M. Anlage, The physics and applications of superconducting metamaterials, J. Opt. **13**, 02400 (2011).

[35] Q. Zhao, L. Kang, B. Du, H. Zhao, Q. Xie, X. Huang, B. Li, J. Zhou, and L. Li, Experimental Demonstration of Isotropic Negative Permeability in a Three-dimensional Dielectric Composite, Phys. Rev. Lett. **101**, 027402 (2008).

[36] J. C. Ginn, I. Brener, D. W. Peters, J. R. Wendt, J. O. Stevens, P. F. Hines, L. I. Basilio, L. K. Warne, J. F. Ihlefeld, P. G. Clem, and M. B. Sinclair, Realizing Optical Magnetism from Dielectric Metamaterials, Phys. Rev. Lett. **108**, 097402 (2012).

[37] X. Liu, Q. Zhao, C. Lan, and J. Zhou, Isotropic Mie resonance-based metamaterial perfect absorber, Appl. Phys. Lett. **103**, 031910 (2013).

[38] A. G. Webb, Dielectric materials in magnetic resonance, Concepts Magn. Reson. **38A**, 148 (2011).

[39] J. Wang, S. Qu, Z. Xu, J. Zhang, H. Ma, Y. Yang, and C. Gu, Broadband planar left-handed metamaterials using split-ring resonator pairs, Photonics Nanostruct. Fundam. Appl. **7**, 108 (2009).

[40] U. Katscher, P. Bornert, C. Leussler, and J. Van Den Brink, Transmit sense, Magn. Reson. Med. **49**, 144 (2003).

[41] Y. Zhu, Parallel excitation with an array of transmit coils, Magn. Reson. Med. **51**, 775 (2004).